TECHNOLOGY

A thermoreversible, photocrosslinkable collagen bio-ink for free-form fabrication of scaffolds for regenerative medicine

Kathryn E. Drzewiecki, Juilee N. Malavade, Ijaz Ahmed, Christopher J. Lowe, and David I. Shreiber

As a biomaterial, collagen has been used throughout tissue engineering and regenerative medicine. Collagen is native to the body, is highly biocompatible, and naturally promotes cell adhesion and regeneration. However, collagen fibers and the inherent weak mechanical properties of collagen hydrogels interfere with further development of collagen as a bio-ink. Herein, we demonstrate the use of a modified type-I collagen, collagen methacrylamide (CMA), as a fibril-forming bio-ink for free-form fabrication of scaffolds. Like collagen, CMA can self-assemble into a fibrillar hydrogel at physiological conditions. In contrast, CMA is photocrosslinkable and thermoreversible, and photocrosslinking eliminates thermoreversibility. Free-form fabrication of CMA was performed through self-assembly of the CMA hydrogel, photocrosslinking the structure of interest using a photomask, and cooling the entire hydrogel, which results in cold-melting of unphotocrosslinked regions. Printed hydrogels had a resolution on the order of ~350 μm, and can be fabricated with or without cells and maintain viability or be further processed into freeze-dried sponges, all while retaining pattern fidelity. A subcutaneous implant study confirmed the biocompatibility of CMA in comparison to collagen. Free-form fabrication of CMA allows for printing of macroscale, customized scaffolds with good pattern fidelity and can be implemented with relative ease for continued research and development of collagen-based scaffolds in tissue engineering.

***Keywords*: 3D Printing; Bioprinting; Tissue Engineering; Methacrylamide; Methacrylated; Hydrogel.**

INNOVATION OF THE TECHNOLOGY

This pioneering study demonstrates the first use of collagen methacrylamide as a bio-ink for simple free-form fabrication of patient-specific scaffolds. Unlike many other collagen bio-inks used for 3D printing, scaffolds printed with CMA retain their fibrillar nature, which mimic fibers found in the body and present natural epitopes to cells. Further, due to photocrosslinking, CMA scaffolds are mechanically stronger and easier to handle, resolving a common problem faced when using biological materials in 3D printing. While CMA can be used in the future with nozzle-based or stereolithography 3D printers, this study demonstrates the ease of free-form fabrication with CMA using common equipment found throughout laboratories in the world, including UV light sources, refrigerator and incubator. This innovative, rapid, low-cost method utilizing CMA as a bio-ink enables many labs to partake in 3D printing of collagen-based, patient-specific scaffolds.

INTRODUCTION

Solid free-form fabrication and 3D printing have vastly improved the ease and speed of customizing and producing patient-specific scaffolds in medicine at relatively low cost[1–6]. Although 3D printing platforms and speed in printing have progressed[6,7], there is a significant lack of diversity of printable biomaterials that have both desirable properties for printing and necessary properties for implantation[2,8]. Successful 3D printing approaches will comprise a 3D printing platform that is affordable, scalable, and versatile to many bio-inks, and bio-inks that are biocompatible, biodegradable, and exhibit proper mechanical and bioactive tissue mimicry[2,8–10].

Type-I collagen, the major protein constituent of soft tissue, is a natural choice as a base material for tissue engineering, as it supports cell adhesion, differentiation, and other natural processes[11], is native to many tissues throughout the body, and is a primary component of the body's own regenerative approach during wound healing[12]. In one of the first clinically approved applications of tissue engineering, collagen was formulated as an extensively crosslinked freeze-dried sponge for covering and healing deep wounds resulting from burn injury[13]. Collagen sponge wound coverings prevented foreign substances from entering the wound site, and promoted cellular infiltration at the injury site to facilitate new tissue growth and remodeling[13,14]. Most recently, FDA approval was granted for collagen membranes seeded with autologous chondrocytes for cartilage regeneration[15,16]. While the applications of collagen as sponges in tissue engineering are extensive, its uses in solid free-form fabrication or 3D printing applications to create hydrogels or sponges in defined 2D and 3D geometries is limited. Without considerable crosslinking, type-I collagen has relatively weak mechanical properties and is difficult to handle or fabricate compared to competing synthetic or modified polymers[17].

Department of Biomedical Engineering, Rutgers, The State University of New Jersey, 599 Taylor Road, Piscataway, NJ 08854, USA. Correspondence should be addressed to D.I.S. (shreiber@soe.rutgers.edu).

Received 22 May 2017; accepted 14 August 2017; published online 17 October 2017; doi:10.1142/S2339547817500091

Type-I collagen forms highly ordered D-banded fibers at physiological conditions that are vital for the natural presentation of bioactive epitopes and for providing anisotropic strength and stiffness, and it requires high concentrations or crosslinking to match properties of tissues[18,19]. These properties can significantly complicate 3D printing when using collagen as bio-ink, especially forms of nozzle-based 3D printing[18–21]. Alternatively, type-I collagen can be cast in specific geometries, but this requires the use of a negative mold to construct the tissue of interest[3,4,22], which can delay treatment for the patient due to increased processing times for scaffold customization, a major benefit of 3D printing.

Despite these difficulties, there have been many attempts with varying degrees of success in using collagen as a bio-ink for 3D printing or solid free-form fabrication. Some of these techniques include multiphoton crosslinking[23], extrusion[24,25], and inkjet bioprinting[26–28]. Many of these methods utilize materials in addition to collagen when 3D printing, such as polycaprolactone and alginate, to generate constructs with improved mechanical integrity[25,27]. Type-I collagen has been used alone as a bio-ink in different 3D printing strategies. In one of the earliest examples, a direct-write bioassembly system was used to extrude type-I collagen with and without cells in controlled patterns with good pattern fidelity and cell viability, but structures failed to maintain mechanical integrity if time for fibrillogenesis was cut short[29]. A custom, nozzle-based 3D printing system used lyophilized and rehydrated collagen sponges as bio-ink where printed scaffolds had spatial resolution on the order of 500 μm[30]. In another method called freeform reversible embedding of suspended hydrogels (FRESH), a MakerBot Replicator was modified to use a syringe-based extruder to release collagen bio-ink into a HEPES and gelatin slurry bath; viscosity differences between solutions allowed for structural maintenance of the printed collagen while proper pH and temperature control promoted self-assembly of the collagen hydrogel in the shape of the printed structure, which had a resolution on the order of 200 μm[31]. Though relatively low cost, many of these methods have associated complexities with set-up and issues with nozzle-based printing as previously mentioned, namely nozzle clogging with collagen hydrogel suspension[21, 31].

Another popular approach to 3D printing involves photoreactive bio-inks, such as acrylated polymers, which allow for the conversion of a liquid to a semi-solid gel by controlled exposure to free radicals via a photoinitiator and light with matched wavelength (usually UV). A nozzle-based 3D printer with modification for UV treatment is capable of printing cell-laden, methacrylated gelatin constructs in controlled architectures, such as lattices and hollow fibers[32]. Similarly, laser-polymerized hydrogel structures can be produced layer-by-layer using the polymer poly(ethylene glycol) diacrylate when specific regions are exposed to UV light in modified stereolithography apparatuses[33,34]. However, these approaches cannot be performed with collagen, which is not photoreactive and requires ordered, temperature-dependent self-assembly to promote the formation of natural D-banded fibers.

We have developed a methacrylate-derivatized type-I collagen — collagen methacrylamide (CMA) — that retains the ability to form D-banded fibrillar hydrogels[35,36]. CMA has two unique properties that allow for free-form fabrication: 1) following fibrillogenesis, CMA can be photocrosslinked using a photoinitiator and UV light to stiffen the hydrogel where it is exposed to light[35], and 2) fibrillogenesis of CMA is thermoreversible — it can reversibly cycle between liquid and fibrillar hydrogel states when cycled between 4 °C and 37 °C[36]. Importantly, photocrosslinking eliminates thermoreversibility. Together, these properties allow for simple free-form fabrication of CMA to construct fibrillar, customized, collagen-based scaffolds for regenerative medicine. This method is distinct from solid free-form fabrication, as it does not require the production of a negative mold for fabrication, reducing times for scaffold customization. Further, in comparison to many 3D printing or free-form fabrication techniques, this method is very easy to implement, merely requiring CMA, a UV light source, and laser-printed transparencies for photopatterning.

In this paper, we describe the method for free-form fabrication of CMA, the resolution of printing, the construction of photopatterned hydrogels and scaffolds, and the ease of creating cell-laden, printed hydrogels. We also evaluate the biocompatibility of CMA *in vivo*. The ease of implementation of this free-form fabrication strategy and use of CMA as a collagen-based bio-ink present many opportunities for scaffold customization of a collagen-based material to further applications of collagen in regenerative medicine.

MATERIALS AND METHODS

CMA hydrogel preparation

Type-I collagen (Elastin Products Company, C857, Owensville, MO) was reconstituted in 0.02 M acetic acid at 3.75 mg/mL. CMA was synthesized from the solubilized type-I collagen in the method outlined in Gaudet *et al.*[35] and was also reconstituted in 0.02 M acetic acid at 3.75 mg/mL. For free-form fabrication, unless otherwise stated, CMA was buffered on ice according to the following formula: 20 μL 1 M HEPES (H3537, Sigma-Aldrich, St. Louis, MO), 134 μL 0.15 N NaOH (S2770, Sigma-Aldrich), 100 μL 10X PBS (P5493, Sigma-Aldrich), 59 μL 1X PBS (860454, Thermo Fisher Scientific, Waltham, MA), 10 μL 10% Irgacure (I2959, a gift from Ciba Specialty Chemicals) solubilized in neat methanol, and 677 μL CMA. Hydrogels were always prepared to a final concentration of 2.5 mg/mL and pH 7 unless otherwise specified. Buffered CMA was plated in 14 mm glass-bottomed MatTek dishes (P35G-0-14-C, MatTek Corporation, Ashland, MA) and self-assembled for one hour (unless otherwise stated) at 37 °C to create CMA hydrogels. All samples exposed to UV were plated in MatTek dishes.

Photomask design

Two classes of photomasks were employed for the photolithographic approach to free-form fabrication. Low resolution photomasks of larger, defined shapes were designed in Microsoft PowerPoint and printed on transparencies using a commercial laser printer. These masks were used for free-form fabrication unless otherwise stated. Separate high resolution photomasks were designed as grids of defined line widths and line spacings ranging from 0.25 mm to 1.0 mm and 1.0 mm to 2.5 mm respectively. These high resolution photomasks were designed in AutoCad and printed by CAD/Art Services, a service that can print photomask features on the order of 10 μm in resolution (Bandon, OR).

Free-form fabrication of CMA

Self-assembled CMA hydrogels in MatTek dishes were photocrosslinked using UV light (365 nm, 100 mW/cm^2). Parallel plate rheology during UV exposure was used to determine the exposure time for each batch of CMA and for a particular volume (**Supplementary Fig. 1**). An X-Cite 120 PC light source and light guide were used (Excelitas Technologies Corp., Waltham, MA) (**Fig. 1**), though any UV light source will work (**Supplementary Fig. 2**). The light passed through a UV bandpass filter and quartz glass plate before reaching the bottom of the MatTek dish. To photopattern specific regions of the CMA hydrogel, a laser-printed transparency was placed between the MatTek dish and quartz glass bottom plate. Exposed CMA samples were cold-melted on pre-cooled aluminum plates at 4 °C for 10 minutes. CMA that was not exposed to UV light (referred to as unphotocrosslinked CMA) disassembled and was removed through dilution with cold PBS and gentle agitation. Photopatterned hydrogels were imaged using an Aven Digital Handheld Microscope (26700-302, Aven Inc. Ann Arbor, MI), a USB digital microscope, using a 10X objective unless otherwise specified.

Spatial resolution of free-form fabrication

A 100 μL volume of CMA suspension formulated as described was plated in the MatTek dishes, allowed to self-assemble (final height ~600 μm), and

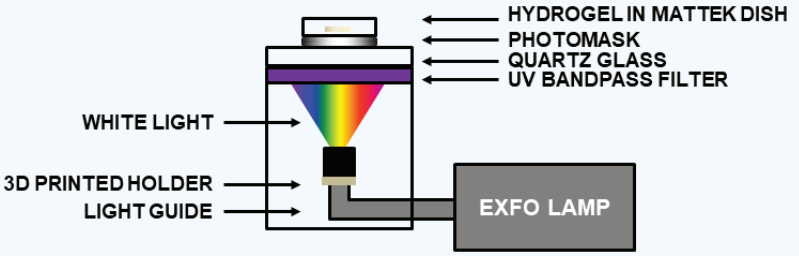

Figure 1 UV Photocrosslinking Set-Up for CMA Free-Form Fabrication. Light was filtered to allow UV to photocrosslink the sample using a photomask. Without a photomask, samples will be fully exposed to UV light, which results in complete photocrosslinking of the entire hydrogel.

photocrosslinked through the high resolution photomasks for 45 seconds. The area and shape of the voids or regions of unphotocrosslinked CMA that cold-melted were measured and compared to the grid pores in the photomask[37]. Circularity measurements (Equation 1) were performed to quantify the rounding of corners from the ideal square (circularity of ~0.78) in the mask:

$$\text{Circularity} = 4\pi\ (\text{Area}/\text{Perimeter}^2) \quad (1)$$

The pores in the photopatterned hydrogels and photomasks were traced using the Polygon Selections Tool in ImageJ (NIH, Bethesda, MD). Pores at the edges of the hydrogel were not measured. Five different hydrogels were photopatterned with each photomask, and the average pore area and circularity measurement obtained for the set of five was reported.

The width of patterned lines was measured from changes in pixel intensity in a linear region taken across the sample[38]. After aligning images of the mask and sample, a line of constant length was drawn in both images in the exact plane, and the Plot Profile function in ImageJ was used to identify the intensity value as a function of position along the line. A moving-average filter was applied to smooth the pixel intensity value curves.

Spatial resolution of CMA sponges created through free-form fabrication

Buffered CMA (400 μL) was plated in MatTek dishes, self-assembled (final height ~2.5 mm), and photocrosslinked through a photomask for two minutes. Following cold-melting and removal of unphotocrosslinked CMA, hydrogels were frozen at –80 °C for three hours and lyophilized overnight to create freeze-dried scaffolds. Scaffolds were re-hydrated with PBS for one hour. Scaffolds (n = 5 for each state) were imaged at each stage of the process using an Aven Digital Handheld Microscope and compared to the photomask using the Polygon Selections Tool in ImageJ.

Free-form fabrication of cell-encapsulated hydrogels

Adult human mesenchymal stem cells (hMSC) (Institute for Regenerative Medicine, Texas A&M College of Medicine, item# 8013L) were cultured in hMSC media composed of MEM-alpha (12561-049, Thermo Fisher Scientific), 10% fetal bovine serum (S11550, Atlanta Biologicals, Flowery Branch, GA), 1% Penicillin/Streptomycin (P/S) (P4458, Sigma-Aldrich), 1% L-glutamine (G7513, Sigma-Aldrich), and 1 ng/mL bFGF (100-18B, Peprotech, Rocky Hill, NJ). Cells were encapsulated in buffered hydrogel suspensions at ~150,000 cells/mL. Self-assembly entrapped the cells within the hydrogel. CMA for cellular hydrogels was formulated as described, but 10X MEM (M0275, Sigma-Aldrich) and Medium 199 (M199) (12350-039, Thermo Fisher Scientific) were used instead of 10X PBS and 1X PBS, respectively. The amount of M199 was reduced by 30 μL, and 10 μL of L-glutamine, 10 μL of P/S, and 10 μL of 1 M ascorbic acid (255564, Sigma-Aldrich) in M199 were added. Ascorbic acid was used to temper the effect of free radicals on cells[39–41], and its addition had no effect on pattern fidelity (**Supplementary Fig. 3**). Buffered CMA with cell suspensions were plated in MatTek dishes (200 μL). Free-form fabrication of the cell-laden hydrogels was performed as described above. Photopatterned CMA hydrogels (final height ~1.2 mm) were exposed to UV for 25–30 seconds through a photomask. All samples were cold-melted for 10 minutes and rinsed with cold hMSC media to remove unphotocrosslinked material. Samples were then rinsed with 2 mL of warm media for 15 minutes and incubated in fresh warmed media (2 mL) at 37 °C, 5% CO_2 for 24 hours. To assess cell viability, samples were stained using calcein-AM from the LIVE/DEAD Viability/Cytotoxicity kit (L3224, Thermo Fisher Scientific) and imaged using a 4X objective with an Olympus IX81 fluorescence microscope (488 nm excitation, 520 nm emmision). Samples were also imaged with the Aven Digital Handheld Microscope to evaluate hydrogel shape and size.

Cytotoxicity was evaluated by preparing cellular CMA and collagen gels with and without Irgacure, where the volume of Irgacure was replaced with M199. Select samples (final height ~1.2 mm) were exposed to UV light. Samples were self-assembled, fully exposed to UV, and placed at 4 °C for 10 minutes for cold-melting. CMA samples that disassembled because they were not exposed to UV with Irgacure were re-assembled at 37 °C for 15 minutes. Samples were rinsed with warmed media once and incubated in fresh media at 37 °C, 5% CO_2 for 24 hours. Cell viability was evaluated using a LIVE/DEAD Viability/Cytotoxicity kit. Three Z-stacks of each sample were taken at random positions using a 10X objective in 100 μm increments for a total depth of 1000 μm using an Olympus IX81 fluorescence microscope with filters at 488 nm and 568 nm. Z-stacks were pseudo-colored (live – green, dead – red), merged using ImageJ software, and the Z Project function (Max Intensity) was used to create a 2D image. Live and dead cells were counted using the Cell Counter Plugin. Data is reported as the average of three separate experiments with three samples in each condition per experiment.

In vivo biocompatibility studies

The biocompatibility of CMA and photocrosslinked CMA hydrogels was compared to type-I collagen control hydrogels using a subcutaneous implantation study in rats. For each of the three conditions, disk-shaped samples (9.5 mm diameter, 3.0 mm height) were prepared. Collagen and CMA suspensions were prepared similar to cell-encapsulated hydrogels, but without Irgacure or ascorbic acid, supplementing the remaining volume with M199. A 200 μL sample of buffered suspension was plated within polydimethylsiloxane (PDMS) rings in small Petri dishes to form hydrogels that were 9.5 mm diameter and 3.0 mm in height. Photocrosslinked CMA hydrogels were made using the free-form fabrication method. Photocrosslinked CMA hydrogels were prepared with Irgacure, but without ascorbic acid. These suspensions were plated in MatTek dishes (432 μL), self-assembled, and photocrosslinked using a photomask of a circle with a diameter of 9.5 mm to create hydrogels of the same height and diameter of the collagen and CMA plated in PDMS molds. Exposure time was increased to two minutes. Photocrosslinked CMA was cold-melted and rinsed with sterile PBS to remove cold-melted CMA and obtain the appropriately sized hydrogels for implantation.

All procedures were conducted in accordance with approved protocols from the Institutional Animal Care and Use Committee (IACUC). Male Sprague-Dawley rats (SD, Charles River Laboratories, Wilmington, MA, 300 g–350 g, age 3–4 months) were anesthetized with 5% isoflurane gas. The backs of the rats were shaved and disinfected. During surgery, anesthesia was maintained with 1–2% isoflurane gas. An incision was

made vertically along the length of the rat. Pockets ~3 mm deep were created at two sites on each side of the midline approximately 5 cm apart for a total of four implantation sites per animal. One hydrogel was subcutaneously implanted in each pocket. The incision was closed with a single staple. A total of six rats were used — three were evaluated at the 1-week timepoint and three were evaluated at the 6-week timepoint. With four implant sites per animal and three types of gels (collagen, CMA, and photocrosslinked CMA), there were 12 samples total at each timepoint, or four for each gel type. Hydrogels were randomly assigned to the implant sites, with each animal receiving at least one implant of each type. After 1 or 6 weeks, rats were euthanized via carbon dioxide asphyxiation. The tissue was explanted, capturing the remaining scaffold when observable, and was fixed in 4% paraformaldehyde for 1 week.

Fixed samples were embedded in OCT compound, frozen, and sectioned transversely into 40 μm sections. Sections were stained with hematoxylin and eosin (H&E) and imaged using a VS120 Color Microscope with a 40X objective. Separate sections were stained immunohistochemically using a mouse anti-rat type-I collagen antibody (clone 1F10C2, 7043, Chondrex, Inc., Redmond, WA) at a 1:500 dilution and a rabbit anti-bovine type-I/type-III collagen antibody (2150-2305, Bio-Rad, Raleigh, NC) at a 1:100 dilution, followed with secondary antibodies of goat anti-mouse AlexaFluor647 (A-11008, Thermo Fisher Scientific) and goat anti-rabbit AlexaFluor488 (A-21235, Thermo Fisher Scientific) at 1:500 dilution. A DAPI stain was applied during mounting (D3571, Thermo Fisher Scientific). Immunohistochemically stained sections were imaged using an Olympus IX81 fluorescence microscope with a 4X objective. ImageJ software was used to pseudo-color and overlay images taken in each channel.

Statistical analysis

Photopatterned samples were compared to the photomask using a Student's *t*-test with the area and circularity of the photomask as the test statistic. Data from the sponge spatial resolution study (area) were analyzed using a Student's *t*-test in comparison to the photomask as the test statistic, and a one-way ANOVA among the scaffold types followed by post hoc pairwise comparisons with Tukey's All Pairs Comparisons was performed. Data from the cytotoxicity study were analyzed using a one-way ANOVA followed by post hoc pairwise comparisons with Tukey's All Pairs Comparisons. For all statistical analysis, differences were considered significant at $p < 0.05$.

RESULTS

Free-form fabrication of CMA hydrogels is accurate to ~350 μm

Spatial resolution was assessed following exposure through photomasks with a range of line widths (0.25 mm–1.0 mm) and line spacings (1.0 mm and 2.5 mm) (**Fig. 2a**). Hydrogels photopatterned with the 1.0 mm width and 2.5 mm spacing photomask had the best pattern fidelity when compared to the photomask measured via area and circularity (**Fig. 2b,c**). CMA hydrogels photopatterned with 0.25 mm width and 1.0 mm spacing had the lowest pattern fidelity, with an average of 50% over-photocrosslinking in the photomask pore area (**Fig. 2b**). The area of the cold-melted regions in the CMA hydrogels was always statistically lower than the corresponding area of the photomask. Circularity measurements demonstrated a slightly different trend — hydrogels patterned with 1.0 mm width and 1.0 mm spacing best matched the square-shaped pores (circularity measurements of ~0.88 vs. ~0.78, respectively) (**Fig. 2c**). Spacing above 1.0 mm resulted in gels that were similar in circularity. However, as the line width decreased below 1.0 mm, the circularity increased. Circularities for all photopatterned hydrogels were statistically higher than the photomask circularity, suggesting that excess free radicals diffused away from areas of light exposure. Pixel intensity measurements in photopatterned CMA-photomask overlays demonstrated accuracy in photocrosslinking when examining regions exposed to UV light and the photomask (**Fig. 3**). Some regions of excess photocrosslinking can be seen in the overlaid images. Consistent with the previous measurements, over-photocrosslinking increased as the line width decreased. Overall, although there were significant differences between the photomask and photocrosslinked hydrogel, particularly at line widths and spacings below 1.0 mm, the method produced photopatterned hydrogels with similar pattern fidelity to the photomask at 2.5 mm width and 1.0 mm spacing. Based on the amount of over-photocrosslinking in the smallest photomasks, we have a printing resolution of approximately 350 μm.

Free-form fabrication can be used to produce customized sponges

CMA hydrogels were subject to free-form fabrication to create customized CMA hydrogels (**Fig. 4a,b**). Samples were subsequently lyophilized and rehydrated to determine the spatial resolution of samples subject to post-processing steps, such as those involved in making a collagen "sponge" (**Fig. 4c,d**). Photocrosslinked hydrogels maintained good pattern fidelity to the photomask, with no statistically significant differences in area (**Fig. 4e**). Edges in the photocrosslinked hydrogel were more rounded when compared to the photomask (**Fig. 4a,b**). Lyophilized and rehydrated scaffolds were easily handled and maintained pattern fidelity, although they decreased in area by approximately 20% following processing steps (**Fig. 4c–e**). The area of processed scaffolds was statistically smaller than both the area of the photomask and hydrogel (**Fig. 4e**). These results echoed that this simple free-form fabrication method produced hydrogels with good pattern fidelity, and that hydrogels can be subject to post-processing steps to create collagen "sponges" of customized shapes and sizes. Additionally, while this study used a high-intensity light source for photocrosslinking, it is also possible to use hand-held UV light sources for photocrosslinking larger scale (> 5 mm across) scaffolds, albeit with longer photocrosslinking times (**Supplementary Fig. 2**).

Cells remain viable when subject to CMA free-form fabrication

Cells were encapsulated in collagen and CMA scaffolds to evaluate the aspects of free-form fabrication that may affect cell viability. The effects of the photoinitiator, UV treatment, and free radicals on cell viability were each examined. All hydrogels were exposed to cold temperatures for "cold-melting." Additionally, all hydrogels contained ascorbic acid, which was added to temper the effect of free radicals on cell viability[39–41]. Reducing free radical concentration with ascorbic acid did not affect pattern fidelity (**Supplementary Fig. 3**).

Cells demonstrated good viability in all collagen and CMA hydrogels after 24 hours in culture, demonstrating that cells remain viable when subject to the free-form fabrication method (**Fig. 5a**). Collagen hydrogels containing Irgacure that were not exposed to UV had the highest viability (~88%), whereas collagen hydrogels containing Irgacure and that were exposed to UV had the lowest viability (~75%). Collagen hydrogels containing Irgacure that were not exposed to UV had a statistically significant higher proportion of viable cells compared to CMA. This was also seen in collagen and CMA hydrogels without Irgacure that were exposed to UV, indicating that UV exposure alone induces some cell death. In contrast, collagen and CMA hydrogels containing Irgacure that were exposed to UV light were not statistically different, and had the lowest viability overall (~75%). CMA hydrogels containing Irgacure that were not exposed to UV had a significantly higher proportion of viable cells compared to the other CMA conditions. Despite some cell death, a large portion of the cells were viable following all steps of free-form fabrication.

After 24 hours of incubation, the cell-encapsulated, photopatterned CMA hydrogel experienced some cell-mediated compaction due to the high cell density, which was most easily observed in the corners of the hydrogel compared to initial fabrication (**Fig. 5b–d**). Overall, cell-encapsulated CMA hydrogels were photopatterned with good pattern

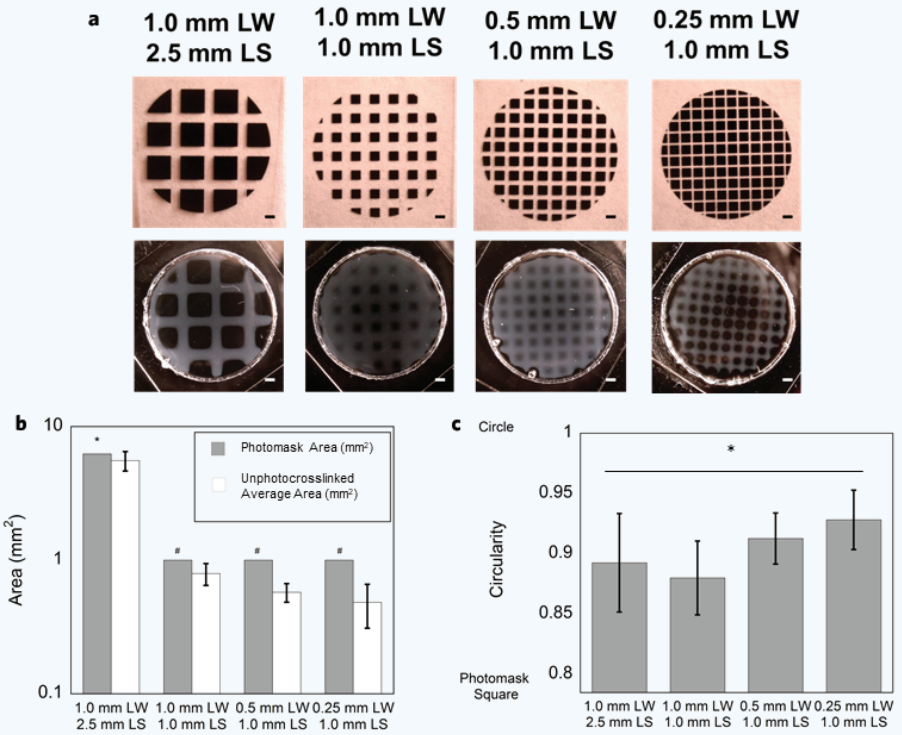

Figure 2 Free-Form Fabrication and Spatial Resolution of Photopatterned CMA Hydrogels to High Resolution Photomasks (a–c). (**a**) Comparison of photomask and photopatterned hydrogel of various line widths (LW) and line spacings (LS) ranging from 0.25 mm–1.0 mm and 1.0 mm to 2.5 mm, respectively. All hydrogels were successfully photopatterned, although the hydrogel with the maximum line spacing (2.5 mm) best reflected the photomask. Pattern fidelity decreased as a function of line width. (**b**) Area of the unphotocrosslinked region was always significantly smaller than the photomask pore ($^{*}p < 0.005$, $^{\#}p < 0.0001$). Regardless, bulk pattern fidelity was still accurate in the 1.0 mm width, 2.5 mm spacing, but then decreased as a function of line width. The 0.25 mm width, 1.0 mm spacing sample had the least pattern fidelity and was ~50% over-photocrosslinked. (**c**) Circularity measurements ranged from ~0.78 (circularity of the photomask pore) to 1 (perfect circle). All photopatterned hydrogels were statistically more circular than the photomask pore, where the 0.25 mm width, 1.0 mm spacing had the largest circularity ($^{*}p < 0.0001$). Scale bar = 1 mm (**a**). Error bars are ± s.d.

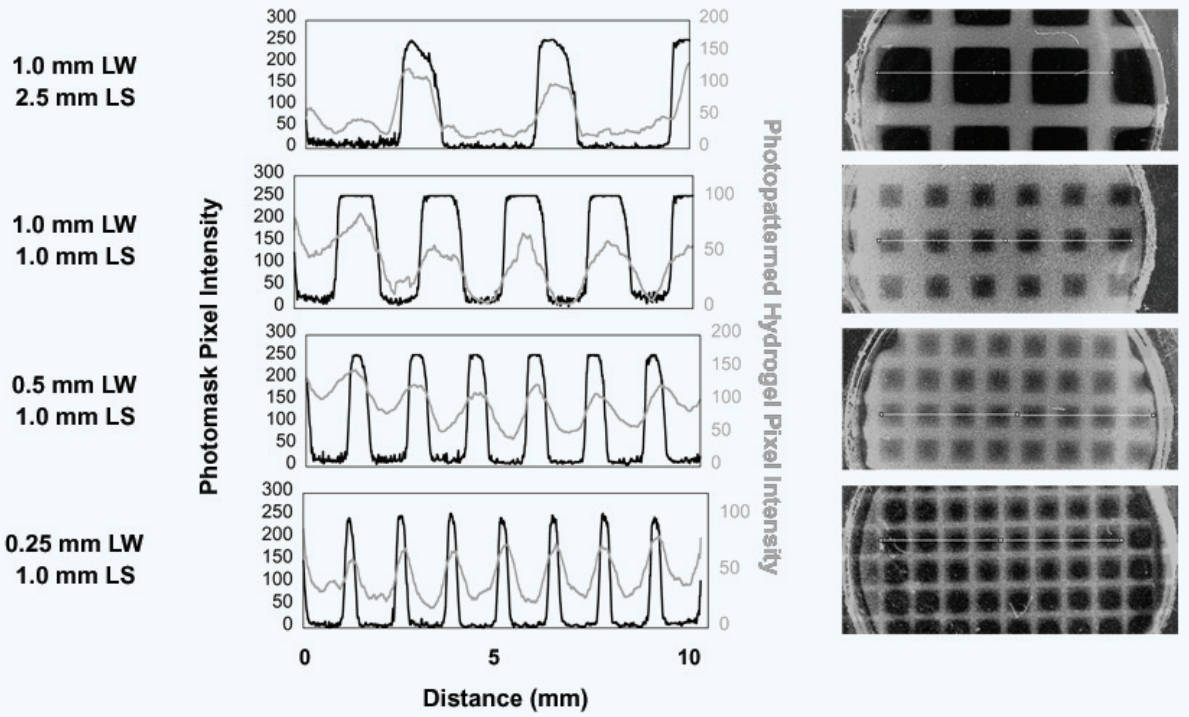

Figure 3 Change in Pixel Intensity across the Photopatterned CMA Hydrogel and High Resolution Photomask. Pixel intensity measurements of photopatterned line widths (LW) and line spacings (LS) across the photopatterned hydrogels were compared to respective intensity changes across the photomask. Overlaid images (**right**) show the tracing for the intensity measurement (**left**) in the photopatterned hydrogel (gray, gray line) and the photomask (black and clear, black line). Evidence of excess free radical production causing over-photocrosslinking can be seen in these images as the rounded corners in the square pore areas of the photomask. All intensity peaks in the photopatterned hydrogels corresponded to the same peaks in the photomask. However, the slope of the change in intensity is lower in photopatterned hydrogels compared to the photomasks, caused by diffusion of free radicals that caused excess photocrosslinking.

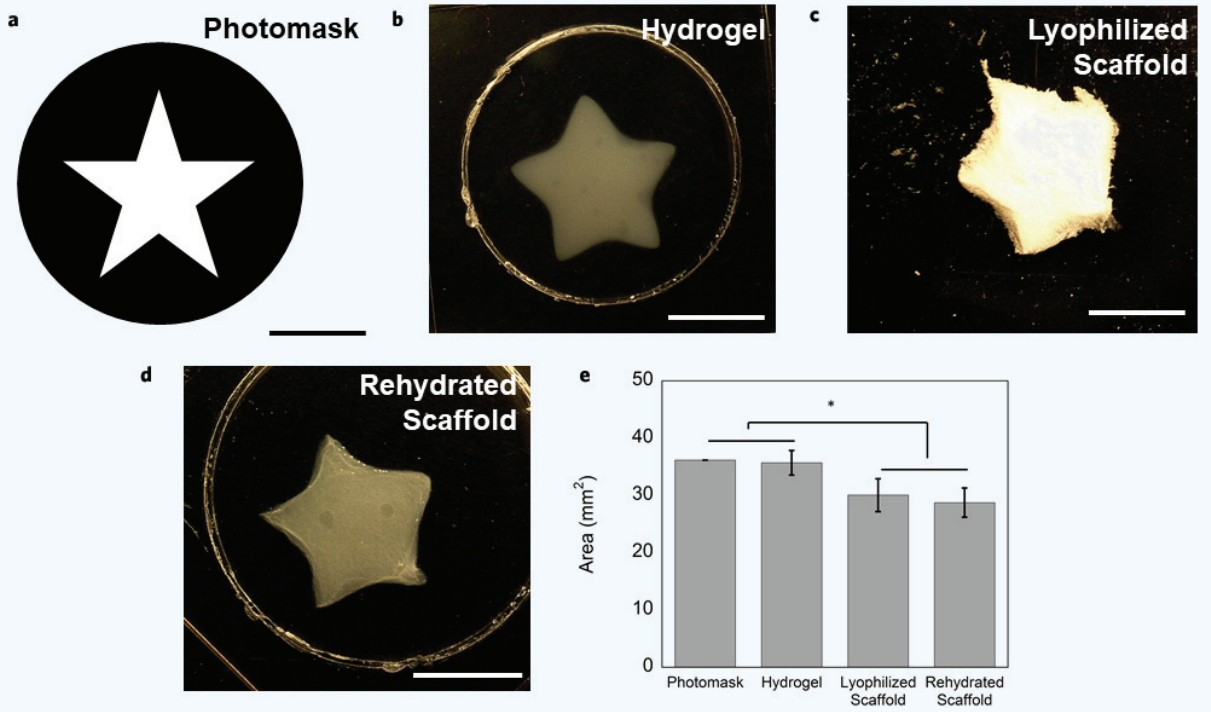

Figure 4 Free-Form Fabrication and Spatial Resolution of CMA Hydrogels, Lyophilized Scaffolds, and Rehydrated Scaffolds (a–e). (**a**) Photomask used to photopattern macroscale, customized CMA hydrogels. (**b**) Representative photopatterned hydrogel exhibited accurate pattern fidelity in comparison to the photomask. (**c,d**) CMA hydrogels can be further processed: hydrogels can be frozen and freeze-dried to create sponges and can be rehydrated as sponges and retain pattern fidelity. (**e**) The CMA hydrogel had the most accurate pattern fidelity compared to the photomask, and there were no significant differences in area between the samples. The area of the lyophilized and rehydrated scaffolds was statistically smaller than the photomask and hydrogel ($^*p < 0.05$). Scale bar = 5 mm (**a–d**). Error bars are ± s.d.

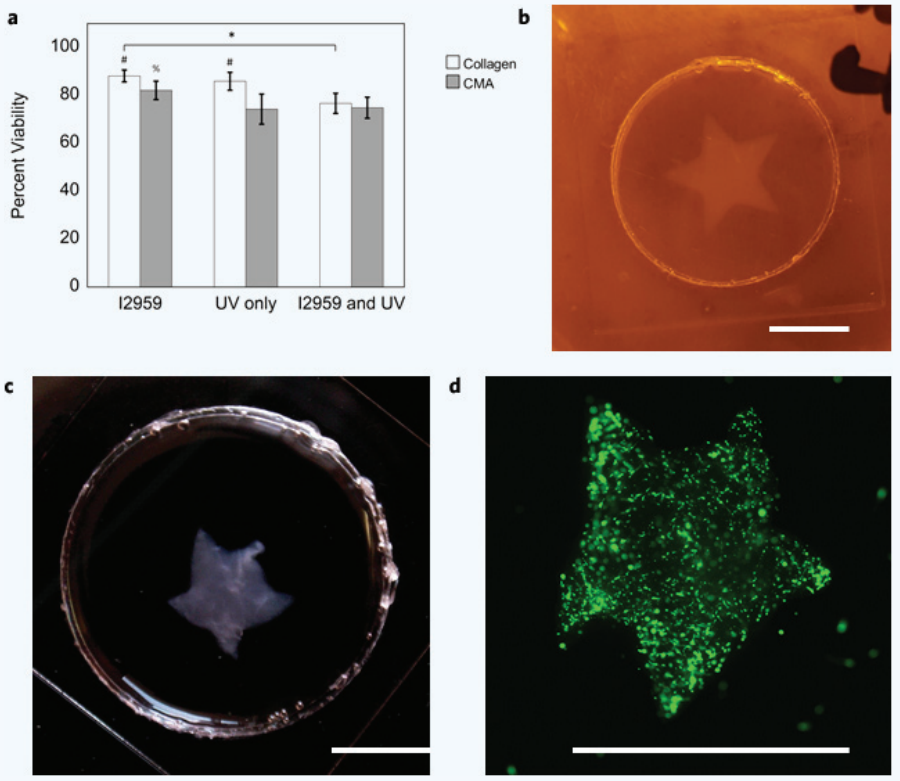

Figure 5 Cytoxicity and Free-Form Fabrication of hMSC-Encapsulated Hydrogels (a–d). (**a**) Cell viability was the highest in collagen hydrogels containing I2959 (~88%), and the lowest in CMA hydrogels with Irgacure and exposed to UV (~75%). Percent cell viability decreased in each condition; hydrogels containing Irgacure had the highest percent viability, and hydrogels containing Irgacure and exposed to UV had the lowest percent viability. These differences were significant when comparing between each collagen hydrogel condition ($^*p < 0.05$); however, CMA hydrogels containing Irgacure and were not exposed to UV had a statistically higher percent viability compared to the other CMA conditions ($^{\%}p < 0.0001$). Cell viability in collagen hydrogels was statistically higher compared to CMA hydrogels, except for the collagen and CMA conditions that contained Irgacure and were exposed to UV ($^{\#}p < 0.0001$). (**b**) Photopatterned, cell-laden hydrogel immediately after cold-melting. (**c**) Photopatterned, cell-laden hydrogel 24 hours after cell culture. (**d**) Calcein-AM stained hMSC in photopatterned CMA hydrogel. All photopatterned, cell-laden hydrogels demonstrated good pattern fidelity as seen in the previous figure (**Fig. 4**). Scale bar = 5 mm (**b–d**). Error bars are ± s.d.

fidelity, similar to the previous set of photopatterned CMA hydrogels from the sponge spatial resolution study (**Fig. 4b,5b**). These data suggest that cells can be subject to free-form fabrication of CMA and maintain viability, allowing for the production of cell-laden, customized hydrogels.

CMA and photocrosslinked CMA are biocompatible

The biological response to CMA hydrogels was compared to the response to type-I collagen, which has been used *in vivo* for wound healing for the past 30 years[13]. Macroscopically, no inflammation was observed at implant sites at either the 1-week or 6-week timepoint. Sectioning proved difficult for such soft tissue even after fixation. In the H&E images seen herein, hydrogels are clearly visible for the collagen and photocrosslinked CMA samples, but only a portion of the hydrogel is present for the CMA hydrogel (**Fig. 6a,b**). Histological analysis showed that all implanted hydrogels at the 1-week timepoint caused an inflammatory response (**Fig. 6a**). A dense layer of cells can be seen surrounding the scaffold with

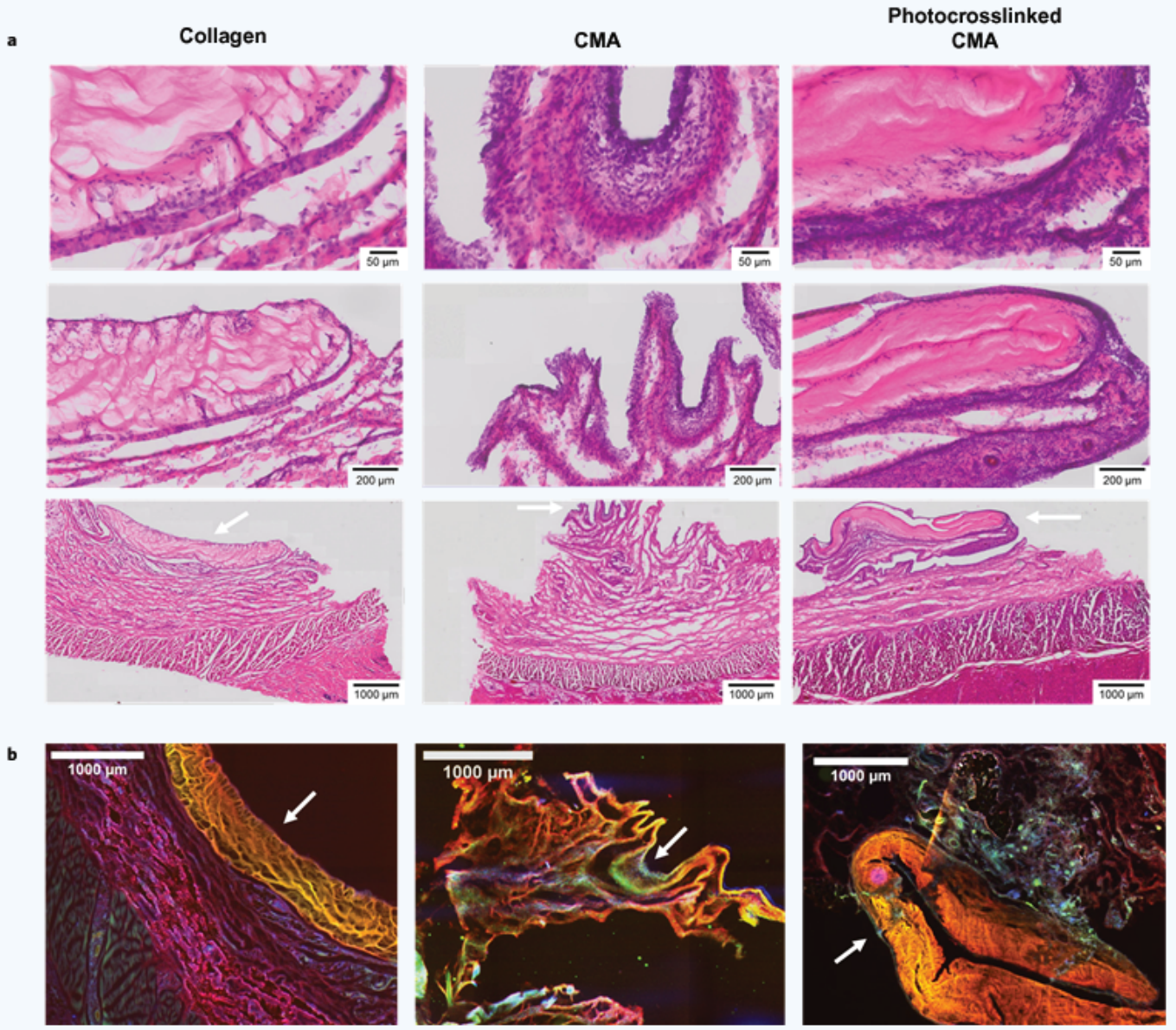

Figure 6 Histology and Immunostaining of Collagen, CMA, and Photocrosslinked CMA Implants 1 Week after Subcutaneous Implantation (a,b). White arrows indicate scaffolds, and all histology images are oriented such that the epidermis is at the bottom of the image and the scaffold is at the top. (**a**) H&E stained sections at the 1-week timepoint of collagen, CMA, and photocrosslinked CMA scaffolds and tissue surrounding the implant site. All samples showed signs of an inflammatory response; the response in the tissue surrounding the collagen implant was more acute compared to that elicited by the CMA and photocrosslinked CMA samples. Cell densities in the CMA and photocrosslinked CMA sections were much higher. Signs of an inflammatory response are seen as cell immigration to the area surrounding the scaffold, with some signs of cell infiltration into the scaffold. (**b**) Immunostaining for rat collagen (red), bovine collagen (yellow), and cell nuclei via DAPI labeling (blue). The rat collagen antibody stained collagen non-specifically; therefore, bovine collagen is seen as yellow in the overlay instead of green. Portions of the collagen and CMA scaffolds were clearly evident in each of the sections (white arrows). DAPI labeling was significant, labeling the immediate area around the scaffold. There was also a high cell density evident in the area surrounding the scaffold, emulating the cell densities seen in H&E staining.

some signs of infiltration. While greater than the response to collagen, the inflammatory response at 1-week to both CMA and photocrosslinked CMA was consistent with a mild reaction to a foreign implant[42]. After 6 weeks, the hydrogels were almost fully degraded (**Supplementary Fig. 4**). Although H&E sections at this timepoint did not contain the hydrogel, some regions of high cell density were still evident, particularly in the CMA hydrogel conditions (**Supplementary Fig. 4**). When compared to the 1-week timepoint, the cell density had subsided some, suggesting that the immune response was resolving.

Sections were also immunostained at the 1-week timepoint where scaffolds were more intact and far less degraded (**Fig. 6b**). The mouse anti-rat type-I collagen antibody demonstrated non-specificity, and dual-stained both the rat and bovine type-I collagen. Therefore, in the overlaid images, bovine collagen is seen as yellow instead of green. The scaffolds are the farthest layer away from the epidermis. Again, the CMA hydrogel was the smallest due to damage during sectioning. All other regions stained for rat type-I collagen. DAPI staining clearly demonstrated a layer of cells surrounding the scaffold. In all samples, a high concentration of DAPI labeling was also seen in the tissue surrounding the hydrogels, suggestive of the immune response seen in H&E staining. Overall, our study indicated CMA and photocrosslinked CMA were biocompatible.

DISCUSSION

CMA is a unique bio-ink derived from a natural biopolymer, type-I collagen. Unlike many other materials used in photolithographic 3D printing applications[32,43–45], photocrosslinking is not required for CMA hydrogel formation. Instead, like collagen, a neutralized CMA suspension forms a fibrillar hydrogel at temperatures above ~20 °C that naturally presents the D-banded structure and biofunctional epitopes. This is distinct from gelatin methacrylate, used throughout 3D printing, which does not retain these important properties that allow the hydrogel or scaffold to more precisely mimic the *in vivo* microenvironment. Collagen self-assembly introduces problems with many 3D printing approaches, specifically those utilizing nozzle-based methods, as collagen fibers can easily clog the nozzle[21,31]. The unique properties of CMA allowed for the development of a nozzle-free, free-form fabrication method with good pattern fidelity through 1) self-assembly of the CMA into a fibrillar hydrogel, 2) photocrosslinking the hydrogel through a photomask, and 3) cooling the hydrogel to cold-melt regions not exposed to UV light. Following wash steps, the customized hydrogel of interest is easily obtained. This entire process can be completed in less than an hour. Cell-laden, photopatterned hydrogels maintain viability through free-form fabrication. Alternatively, cell-free hydrogels can be further processed into collagen sponges, which are used for a variety of applications in tissue engineering.

CMA has strong potential as a bio-ink for rapid production of macroscale, customized collagen-based scaffolds for tissue engineering, but may need more development to generate micron-feature sized hydrogels. Photopatterned CMA hydrogels could be patterned on the order of ~350 μm; smaller line widths and spacings (0.25 mm and 1.0 mm respectively) had lower pattern fidelity compared to the largest spacing (2.5 mm), which best reflected the photomask. Over-photocrosslinking was observed across most of the conditions, as evidenced by the circularity measurements; this was likely due to excess free radicals and/or scattering of the UV light by collagen fibers to expose unwanted regions to light. Larger-scale, photopatterned CMA scaffolds in customized shapes had excellent pattern fidelity when compared to the photomasks. Because we aimed to design an easy method to adapt in any lab for free-form fabrication of a collagen-based bio-ink, we optimized our method for speed and simplicity. However, additional steps can be taken to optimize the photoinitiator concentration, light intensity, and exposure time to obtain hydrogels or scaffolds with better spatial resolution. Other methods for improving pattern fidelity used in other 3D printing techniques include using a collimated light source, free-radical quenchers[46], or inert gas purging[47].

hMSC demonstrated good viability following free-form fabrication, and photopatterned cellular hydrogels retained pattern fidelity after 24 hours in culture. Some cell-mediated compaction occurred in these hydrogels, as can be expected with cell-populated collagen gels[48–53]. Other cells may not be as tolerant of the free-form fabrication process, particularly due to the UV photocrosslinking, which generates free radicals that can be toxic to cells. As we have done in this study, free radical scavengers are often included to attempt to mitigate effects on cells[40,41], provided that the effects of these scavengers on pattern fidelity is evaluated. Previous studies with CMA have demonstrated that cytotoxicity is only observed if the cells are included in the gel during photocrosslinking[54]. No toxicity is observed if cells are seeded on the gels after photocrosslinking and allowed to infiltrate the gel[54]. CMA has also been shown to support viability over longer timepoints, proliferation, and differentiation[35,54]. To further encourage or direct cell infiltration, it is also possible to simultaneously couple acrylated bioactive ligands to CMA during the 3D printing process. Hydrogels can be partially photocrosslinked to prevent thermoreversibility while adding bioactivity, which could be used to promote desired cell infiltration in scenarios where cells are seeded on top of the hydrogel following free-form fabrication. Studies with longer timepoints will focus on cell viability over time to evaluate CMA as a biomaterial for tissue engineering.

In a subcutaneous implant model, we demonstrated that CMA is biocompatible. After 1 week, CMA and photocrosslinked CMA hydrogels elicited a mild immune response that appeared greater than the response to collagen, but not a deleterious response where much higher cell densities and localized cell death occur[55]. After 6 weeks, the immune response had resolved in all cases when comparing the surrounding tissue to that harvested from the 1-week timepoints.

A collagen-based bio-ink has a range of uses throughout tissue engineering, such as made-to-order scaffolds for facial implants, the design of scaffolds for wound healing with pre-patterned internal vasculature, or as a bioactive and structurally functional component of a more complex bio-ink mixture. CMA, like collagen, is promising as a bio-ink: 1) the protein causes minimal immunological reactions, 2) facilitates cell adhesion, and 3) enhances cell attachment and growth[8]. Although both materials retain slow gelation profiles (longer than 10 minutes), CMA can be photocrosslinked to increase mechanical strength of the bioprinted scaffolds[8,35]. The free-form fabrication method described herein using CMA as a bio-ink can produce customized hydrogels within two hours and freeze-dried scaffolds within 24 hours. The method is quite simple, and is easy for academic/government institutions, start-ups, or large biotechnology companies to implement. CMA should also be compatible with other approaches for 3D printing that utilize 3D printers[31], stereolithography[33], or digital projection systems[43, 44]. The properties of CMA should also allow for modified, layer-by-layer 3D printing, which has been accomplished with other materials[33,44]. 3D printing of CMA could be achieved through self-assembly and photocrosslinking the desired structure of interest layer-by-layer. Upon completion, the entire photopatterned hydrogel could be cooled to cold-melt regions of unphotocrosslinked CMA in each layer. Further development of 3D printing methods for CMA could allow for organ printing or complex tissue engineered scaffolds with layer-specific properties.

ACKNOWLEDGMENTS

We thank the New Jersey Center for Biomaterials, in particular Dr. Hilton Kaplan, Derek Wolosyzn, Matthew Richtmyer, and Justin Sotolongo, for their assistance with the animal study. This project was supported in part by the National Institutes of Health [grant number NIH-NINDS 1R01NS078385], Rutgers Neuro Engineering Group, and fellowships from the National Science Foundation [grant numbers NSF DGE

0801620, IGERT on the Integrated Science and Engineering of Stem Cells], Rutgers-UMDNJ Biotechnology Training Program [grant number NIH 5T32GM008339-20], Rutgers Aresty Research Center, New Jersey Commission on Brain Injury Research [grant number CBIR14FEL004], Department of Education Graduate Assistance in Areas of National Need, and a Scholar Award given by the International Chapter of the P.E.O. Sisterhood.

AUTHOR CONTRIBUTIONS

K.E.D. designed and performed research, analyzed data, and wrote the manuscript. J.N.M. performed research, analyzed data, and wrote the manuscript. I.A. designed and performed research and analyzed data, C.J.L. designed and performed research. D.I.S. designed research, contributed analytic tools, and wrote the manuscript. All authors approved the final version of the manuscript.

COMPETING INTERESTS STATEMENT

Rutgers, The State University of New Jersey, holds the patent for the production of collagen methacrylamide, and has executed a non-exclusive license for the technology. D.I.S. is an inventor on the patent, and K.E.D. and D.I.S. receive royalties.

REFERENCES

1. Chia, H.N. & Wu, B.M. Recent advances in 3D printing of biomaterials. *J. Biol. Eng.* **9**, 4 (2015).
2. Guvendiren, M. *et al.* Designing biomaterials for 3D printing. *ACS Biomater. Sci. Eng.* **2**(10), 1679–1693 (2016).
3. Leong, K.F., Cheah, C.M. & Chua, C.K. Solid freeform fabrication of three-dimensional scaffolds for engineering replacement tissues and organs. *Biomaterials* **24**(13), 2363–2378 (2003).
4. Seol, Y.-J., Kang, T.-Y. Kang & Cho, D.-W. Solid freeform fabrication technology applied to tissue engineering with various biomaterials. *Soft Matter* **8**(6), 1730–1735 (2012).
5. Collins, S.F. Bioprinting is changing regenerative medicine forever. *Stem Cells Dev.* **23** (Suppl 1), 79–82 (2014).
6. Zhu, W. *et al.* 3D printing of functional biomaterials for tissue engineering. *Curr. Opin. Biotechnol.* **40**, 103–112 (2016).
7. Murphy, S.V. & Atala, A. 3D bioprinting of tissues and organs. *Nat. Biotechnol.* **32**(8), 773–785 (2014).
8. Hospodiuk, M. *et al.* The bioink: A comprehensive review on bioprintable materials. *Biotechnol. Adv.* **35**(2), 217–239 (2017).
9. Do, A.V. *et al.* 3D printing of scaffolds for tissue regeneration applications. *Adv. Healthc. Mater.* **4**(12), 1742–1762 (2015).
10. Tibbitt, M.W. *et al.* Progress in material design for biomedical applications. *Proc. Natl. Acad. Sci. U.S.A.* **112**(47), 14444–14451 (2015).
11. Kleinman, H.A., Klebe, R.J. & Martin, G.R. Role of collagenous matrices in the adhesion and growth of cells. *J. Cell Biol.* **88**, 473–486 (1981).
12. Martin, P. Wound healing — Aiming for perfect skin regeneration. *Science* **276**, 75–81 (1997).
13. Burke, J.F. *et al.* Successful use of a physiologically acceptable artificial skin in the treatment of extensive burn injury. *Ann. Surg.* **194**(4), 413–428 (1981).
14. Chvapil, M. Collagen sponge: Theory and practice of medical applications. *J. Biomed. Mater. Res.* **11**, 721–741 (1977).
15. Nixon, A.J. *et al.* A chondrocyte infiltrated collagen type I/III membrane (MACI(R) implant) improves cartilage healing in the equine patellofemoral joint model. *Osteoarthr. Cartil.* **23**(4), 648–660 (2015).
16. FDA approves first autologous cellularized scaffold for the repair of cartilage defects of the knee. FDA News Release 2016. Available from: http://www.fda.gov/NewsEvents/Newsroom/PressAnnouncements/ucm533153.htm.
17. Cheung, H.-Y. *et al.* A critical review on polymer-based bio-engineered materials for scaffold development. *Compos. Part B Eng.* **38**(3), 291–300 (2007).
18. Dong, C. & Lv, Y. Application of collagen scaffold in tissue engineering: Recent advances and new perspectives. *Polymers* **8**(2), 42 (2016).
19. Abou Neel, E.A. *et al.* Collagen — Emerging collagen based therapies hit the patient. *Adv. Drug Deliv. Rev.* **65**(4), 429–456 (2013).
20. Bajaj, P. *et al.* 3D biofabrication strategies for tissue engineering and regenerative medicine. *Annu. Rev. Biomed. Eng.* **16**, 247–276 (2014).
21. Gudapati, H., Dey, M. & Ozbolat, I. A comprehensive review on droplet-based bioprinting: Past, present and future. *Biomaterials* **102**, 20–42 (2016).
22. Sachlos, E. *et al.* Novel collagen scaffolds with predefined internal morphology made by solid freeform fabrication. *Biomaterials* **24**, 1487–1497 (2003).
23. Bell, A., Kofron, M. & Nistor, V. Multiphoton crosslinking for biocompatible 3D printing of type I collagen. *Biofabrication* **7**(3), 035007 (2015).
24. Yoon, H. *et al.* Development of cell-laden 3D scaffolds for efficient engineered skin substitutes by collagen gelation. *RSC Adv.* **6**(26), 21439–21447 (2016).
25. Kim, Y. & Kim, G. Collagen/alginate scaffolds comprising core (PCL)–shell (collagen/alginate) struts for hard tissue regeneration: Fabrication, characterisation, and cellular activities. *J. Mater. Chem. B* **1**(25), 3185 (2013).
26. Xu, T. *et al.* Complex heterogeneous tissue constructs containing multiple cell types prepared by inkjet printing technology. *Biomaterials* **34**(1), 130–139 (2013).
27. Pataky, K. *et al.* Microdrop printing of hydrogel bioinks into 3D tissue-like geometries. *Adv. Mater.* **24**(3), 391–396 (2012).
28. Weng, B. *et al.* Inkjet printed polypyrrole/collagen scaffold: A combination of spatial control and electrical stimulation of PC12 cells. *Synthetic Metals* **162**(15–16), 1375–1380 (2012).
29. Smith, C.M. *et al.* Three-dimensional bioassembly tool for generating viable tissue-engineered constructs. *Tissue Eng.* **10**(9/10), 1566–1576 (2004).
30. Nocera, A.D., Salvatierra, N.A. & Cid, M.P. Printing collagen 3D structures. *IFMBE Proc.* **49**, 136–139 (2015).
31. Hinton, T.J. *et al.* Three-dimensional printing of complex biological structures by freeform reversible embedding of suspended hydrogels. *Sci. Adv.* **1**(9), e1500758 (2015).
32. Bertassoni, L.E. *et al.* Direct-write bioprinting of cell-laden methacrylated gelatin hydrogels. *Biofabrication* **6**(2), 024105 (2014).
33. Chan, V. *et al.* Three-dimensional photopatterning of hydrogels using stereolithography for long-term cell encapsulation. *Lab Chip* **10**(16), 2062–2070 (2010).
34. Cha, C. *et al.* Structural reinforcement of cell-laden hydrogels with microfabricated three dimensional scaffolds. *Biomater. Sci.* **2**(5), 703–709 (2014).
35. Gaudet, I.D. & Shreiber, D.I. Characterization of methacrylated type-I collagen as a dynamic, photoactive hydrogel. *Biointerphases* **7**(1–4), 25 (2012).
36. Drzewiecki, K.E. *et al.* Methacrylation induces rapid, temperature-dependent, reversible self-assembly of type-I collagen. *Langmuir* **30**(37), 11204–11211 (2014).
37. Mapili, G. *et al.* Laser-layered microfabrication of spatially patterned functionalized tissue-engineering scaffolds. *J. Biomed. Mater. Res. B Appl. Biomater.* **75**(2), 414–424 (2005).
38. Seidlits, S.K., Schmidt, C.E. & Shear, J.B. High-resolution patterning of hydrogels in three dimensions using direct-write photofabrication for cell guidance. *Adv. Funct. Mater.* **19**(22), 3543–3551 (2009).
39. Fang, Y.Z., Yang, S. & Wu, G. Free radicals, antioxidants, and nutrition. *Nutrition* **18**(10), 872–879 (2002).
40. Williams, C.G. *et al.* Variable cytocompatibility of six cell lines with photoinitiators used for polymerizing hydrogels and cell encapsulation. *Biomaterials* **26**(11), 1211–1218 (2005).
41. Sabnis, A. *et al.* Cytocompatibility studies of an *in situ* photopolymerized thermoresponsive hydrogel nanoparticle system using human aortic smooth muscle cells. *J. Biomed. Mater. Res. A* **91**(1), 52–59 (2009).
42. Anderson, J.M., Rodriguez, A. & Chang, D.T. Foreign body reaction to biomaterials. *Semin. Immunol.* **20**(2), 86–100 (2008).
43. Hahn, M.S., Miller, J.S. & West, J.L. Three-dimensional biochemical and biomechanical patterning of hydrogels for guiding cell behavior. *Adv. Mater.* **18**(20), 2679–2684 (2006).
44. Han, L.H. *et al.* Fabrication of three-dimensional scaffolds for heterogeneous tissue engineering. *Biomed. Microdevices* **12**(4), 721–725 (2010).
45. Nichol, J.W. *et al.* Cell-laden microengineered gelatin methacrylate hydrogels. *Biomaterials* **31**(21), 5536–5544 (2010).
46. Park, S.H. *et al.* Improvement of spatial resolution in nano-stereolithography using radical quencher. *Macromol. Res.* **14**(5), 559–564 (2006).
47. Stansbury, J.W. & Idacavage, M.J. 3D printing with polymers: Challenges among expanding options and opportunities. *Dent. Mater.* **32**(1), 54–64 (2016).
48. Fernandez, P. & Bausch, A.R. The compaction of gels by cells: A case of collective mechanical activity. *Integr. Biol. (Camb.)* **1**(3), 252–259 (2009).
49. Andujar, M. *et al.* Cell migration influences collagen gel contraction. *J. Submicrosc. Cytol. Pathol.* **24**(2), 145–154 (1992).
50. Arora, P., Narani, N. & McCollough, C. The compliance of collagen gels regulates transforming growth factor-beta induction of alpha-smooth muscle actin in fibroblasts. *Am. J. Pathol.* **154**(3), 871–882 (1999).
51. Shreiber, D.I., Enever, P.A. & Tranquillo, R.T. Effects of pdgf-bb on rat dermal fibroblast behavior in mechanically stressed and unstressed collagen and fibrin gels. *Exp. Cell Res.* **266**(1), 155–166 (2001).
52. Shreiber, D., Barocas, V. & Tranquillo, R. Temporal variations in cell migration and traction during fibroblast-mediated gel compaction. *Biophys. J.* **84**, 4102–4114 (2003).
53. Stevenson, M.D. *et al.* Pericellular conditions regulate extent of cell-mediated compaction of collagen gels. *Biophys. J.* **99**(1), 19–28 (2010).
54. Gaudet, I.D. Development, characterization, and applications of self-assembling, photocrosslinkable collagen-based hydrogels. In *Biomedical Engineering* (Rutgers, The State University of New Jersey, New Brunswick, NJ, 2012), p. 310.
55. Anderson, J.M. Soft tissue response. In *Handbook of Biomaterial Properties* (eds.) Black, J. & Hastings, G. (Springer, US, 1998), pp. 490–499.

SUPPLEMENTARY INFORMATION

CMA was buffered according to the method outlined in free-form fabrication of CMA. The mechanical properties of the samples were measured using a Kinexus Ultra Rotational Rheometer (Malvern Instruments, Malvern, UK) with a quartz bottom plate that allowed for photocrosslinking during mechanical testing. A 200 μL sample was loaded in a 600 μm gap between a 20 mm upper geometry and the quartz bottom plate. The temperature of the plate was raised to 37 °C from room temperature at a rate of 10 °C/minute. The sample was self-assembled for a total of 10 minutes, and then the UV light was turned on for two minutes (365 nm, 50 mW/cm^2). The sample was subject to a constant strain rate of 0.5% at 1 rad/s, as the resultant torque was measured over time to acquire the temperature-dependent storage and loss moduli of the hydrogels in shear. The photocrosslinking time for each batch of CMA was determined as the amount of time needed to reach 95% of the maximum storage modulus measured. By reaching this storage modulus, thermoreversibility was prevented. This was measured for each batch of CMA due to lot-to-lot variability in the starting collagen source and the CMA produced, and accounts for the ranges of photocrosslinking times used throughout this study.

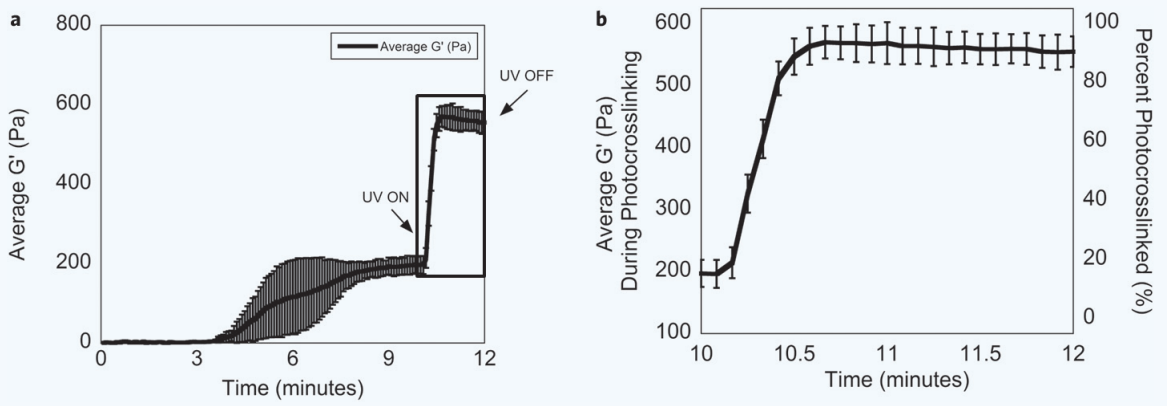

Supplementary Figure 1 Rheological Analysis to Determine Photocrosslinking Time (a,b). (**a**) A typical self-assembly and photocrosslinking curve obtained for CMA, averaged for 3 separately prepared samples of one batch of CMA. The sample began to self-assemble at ~4 minutes when the storage modulus (G′) increased. G′ stabilized over time. The sample was photocrosslinked at the 10 minute timepoint, and G′ further increased. (**b**) The same self-assembly and photocrosslinking curve from 10–12 minutes demonstrated that this particular batch of CMA needed to be photocrosslinked for approximately 25 seconds to reach 95% of the maximum G′. Error bars are ± s.d.

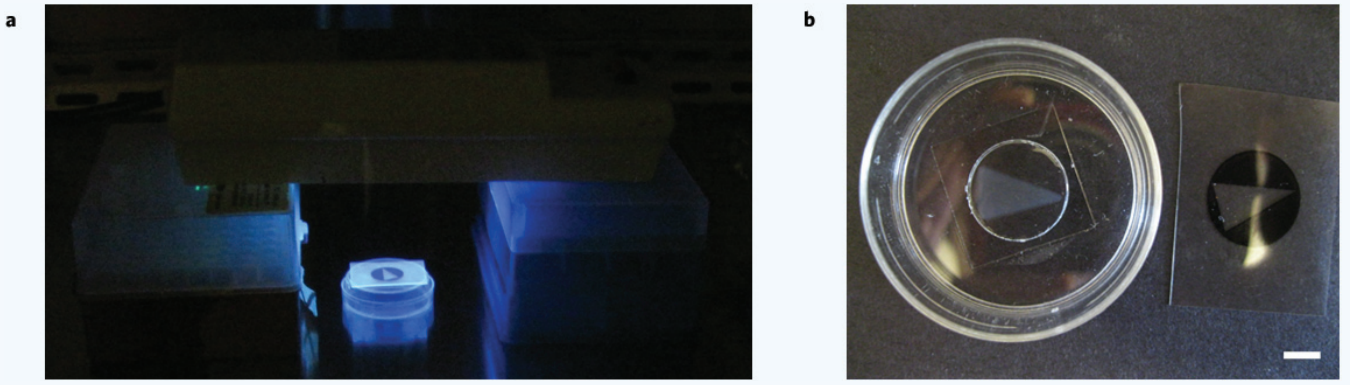

Supplementary Figure 2 Photopatterning CMA Using an Alternate UV Light Source (a,b). (**a**) Photocrosslinking set-up using Blak-Ray Lamp (Model UVL-21, UVP, San Gabriel, CA). Photocrosslinking times were drastically increased using this lamp, as the intensity is much weaker (~8 mW/cm^2). This set-up is top-down, photocrosslinking the sample from above, whereas the set-up used throughout the majority of this study photocrosslinks the sample from below. (**b**) Despite the slower photocrosslinking times, macroscale, photopatterned hydrogels can still be produced with good pattern fidelity. Scale bar = 5 mm.

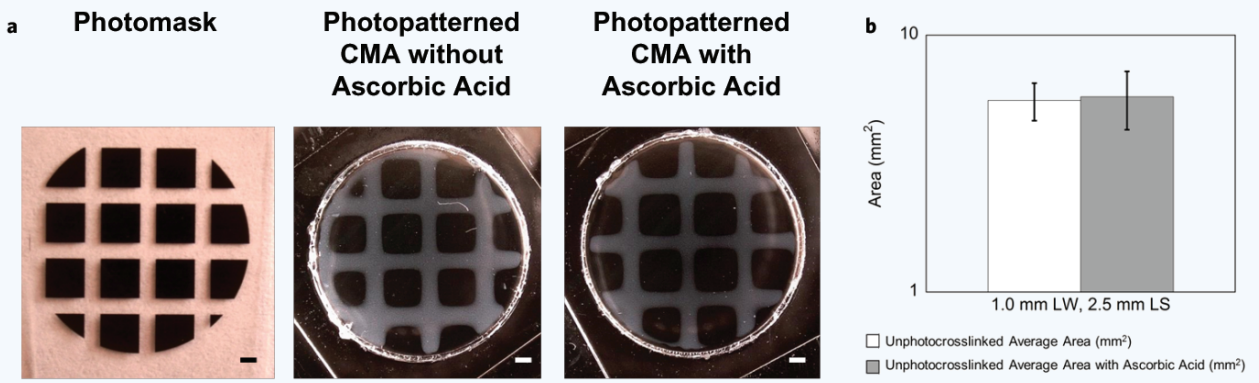

Supplementary Figure 3 Spatial Resolution of Photopatterned CMA with and without Ascorbic Acid (a,b). (**a**) CMA hydrogels photopatterned with and without ascorbic acid demonstrated good pattern fidelity in comparison to the photomask, and were not discernable from one another. (**b**) Area measurements demonstrated no statistical difference between the unphotocrosslinked regions of the hydrogels. Error bars are ± s.d. Scale bar = 1 mm.

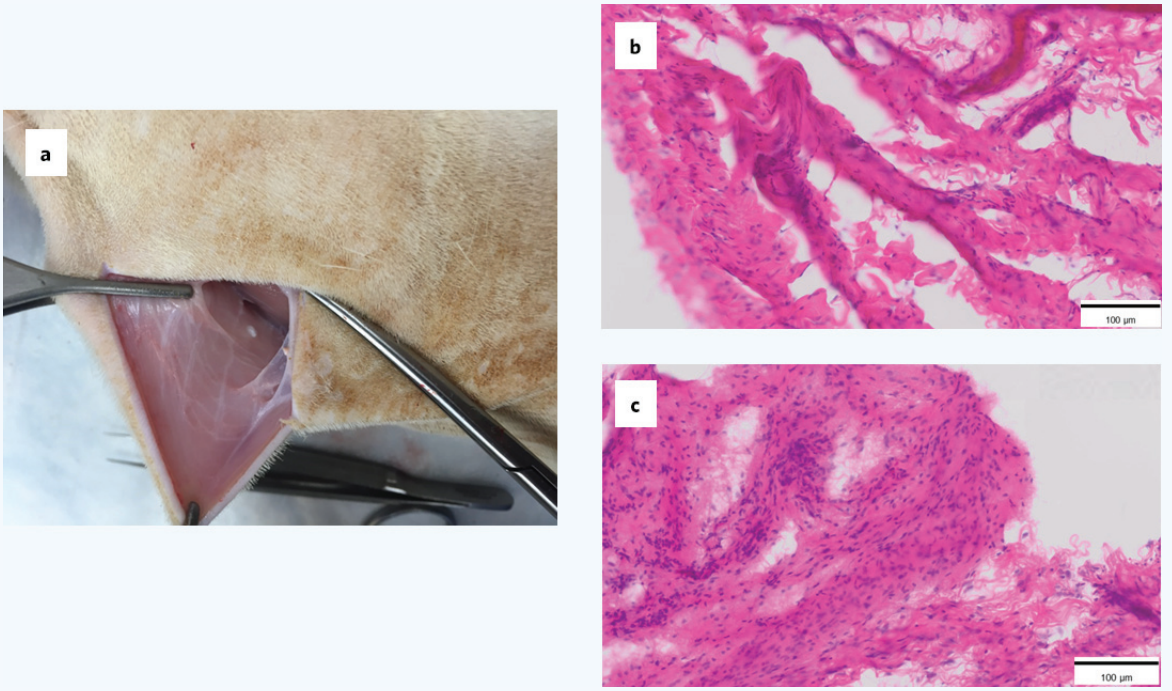

Supplementary Figure 4 Representative Images of Degraded Hydrogel and H&E Stained Sections at the 6-Week Timepoint Post-implantation (a–c). (**a**) Representative image of degraded hydrogel prior to removal. (**b,c**) H&E stained sections of collagen and CMA, respectively. All CMA and photocrosslinked CMA sections showed slightly greater cell density compared to collagen sections, but there were no signs of cytotoxicity in any section. Cell density in all sections had subsided compared to tissue/scaffold explants at 1-week post-implantation.